analytical chemistry

pubs.acs.org/ac Article

In Situ Protease Secretion Visualization and Metastatic Lymph Nodes Imaging *via* a Cell Membrane-Anchored Upconversion Nanoprobe

Yanyun Fang, Yuetong Li, Yuyi Li, Rong He, Yue Zhang, Xiaobo Zhang, Ying Liu,* and Huangxian Ju

Cite This: *Anal. Chem.* 2021, 93, 7258−7265 Read Online

ACCESS | Metrics & More | Article Recommendations | Supporting Information

ABSTRACT: Matrix metalloproteinase (MMP) secretion is highly associated with tumor invasion and metastasis; therefore, monitoring MMP secretion is important for disease progression study and therapy choosing. Though working well for intracellular MMP imaging, the performance of current MMP detection probes is impaired in secretion monitoring due to the diffusion of MMP in an extracellular environment after secretion and low secreted amount. Here, we design a cell membrane-anchored ratiometric upconversion nanoprobe (UCNPs-Cy3/Pep-QSY7/Ab) for *in situ* MMP secretion visualization. Anti-EGFR is functionalized on the nanoprobe to provide specific recognition to tumor cells and guarantee fast response to MMP2 in the local place of secretion. MMP-responsive cleavage of Pep-QSY7 results in Cy3 luminescence recovery at 580 nm, which is ratioed over an internal standard of UCNP emission at 654 nm for MMP2 detection. The presented cell membrane-anchored ratiometric upconversion nanoprobe demonstrated that satisfactory results for *in situ* monitoring of MMP2 secretion from MDA-MB-231 cells and MCF-7 cells, as well as *in vivo* imaging of metastatic lymph nodes, would provide a universal platform for protease secretion study and contribute to tumor invasiveness assessment.

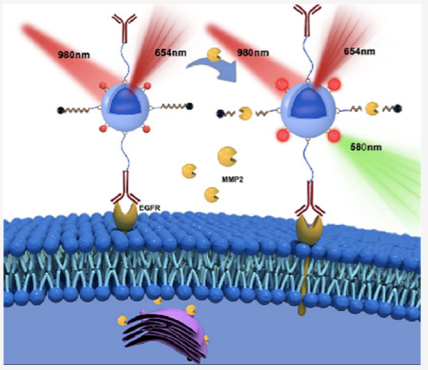

Matrix metalloproteinase (MMP), as one of the zinc- and calcium-dependent proteases, is activated *via* the cellular outward secretion process.[1] It degrades the extracellular matrix and therefore is highly associated with tumor invasion and metastasis.[2−5] Sensitive and accurate monitoring of MMP secretion activity in real-time from living cells indicates small metastatic tumors before conventional imaging or histopathological examination techniques, which helps to understand disease mechanism and perform therapy at early stages.[6−10]

Self-quenching nanoprobes, which covalently link fluorescent dye and quencher molecule at two terminals of the substrate peptide, show fluorescence recovery in response to MMP and have been used for intracellular MMP imaging.[11−13] However, the intracellular MMP expression could not reflect its secretion behavior. Real-time monitoring of MMP secretion has been difficult and rarely reported because of its low abundance as well as the diffusion in the extracellular environment after secretion.[14] Previous extracellular MMP probes collect signal from the culture supernatant of large number cells,[15−17] which compromise the reaction efficiency between detection probes and secreted MMP. Long reaction time is usually required to obtain sufficient detection signal considering the free diffusion of secreted MMP and the random dispersion of detection probes in an extracellular environment. In addition, the diffusion of protease or imaging probes affects secretion detection accuracy. Therefore, the *in situ* imaging of MMP in the local area of secretion is of significant importance.

The cell membrane isolates the living cell and the extracellular environment and therefore is the boundary for all secretion proteases encountering during the outward release process.[18] Installing detection probes on the cell membrane could trap and confine secreted protease in the cellular local area, improve probe and protease interaction, and achieve real-time visualization of protease outward secretion process.[19] The cell membrane has been engineered with polymer patches,[20] DNA strands,[21−24] and small-molecule probes[18,25,26] for detecting cell membrane disturbing molecules and events, but the *in situ* visualization of protease secretion has not been achieved. To design a cell membrane-anchored peptide probe for *in situ* MMP secretion detection, there are two requirements need to be satisfied: (1) the probe anchoring and dynamic imaging process should not affect cell physiological activities and functions and (2) internal standard should be

Received: February 1, 2021
Accepted: April 20, 2021
Published: May 3, 2021

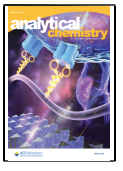

https://doi.org/10.1021/acs.analchem.1c00469
Anal. Chem. 2021, 93, 7258−7265

Scheme 1. Schematic Illustration of (A) Construction of Upconversion Nanoprobe UCNPs-Cy3/Pep-QSY7/Ab and (B) *In Situ* Monitoring of Cell-Secreted MMP2

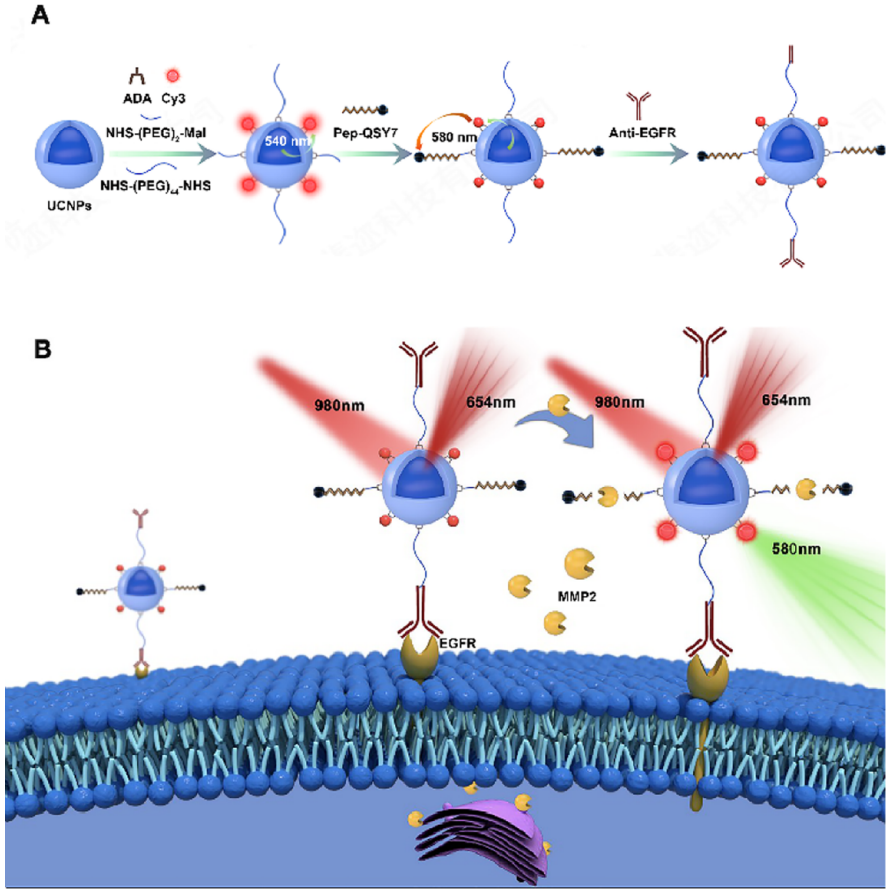

conjugated to probe to calibrate the amount difference of cell membrane-anchored detection probes. Upconversion nanoparticles (UCNPs) are biocompatible, provide adjustable multi-emissions and convenience for surface functionalization, and have been successfully applied in NIR light-controlled spatiotemporally activation of bioimaging and biotherapy.[27−34] Taking advantage of the multiple upconversion emissions under NIR irradiation of UCNPs, here, we developed a cell membrane-anchored ratiometric upconversion nanoprobe for *in situ* monitoring of MMP2 secretion with further application in *in vivo* metastatic lymph node imaging. UCNPs ($NaYF_4$:Gd,Yb,Er@$NaYF_4$) were functionalized with dye Cy3 and MMP2 substrate peptide labeled with QSY7 quencher (Pep-QSY7) at peptide terminus. *Via* Cy3-mediated continuous luminescence resonance energy transfer (LRET) processes, UCNPs emission at 540 nm was quenched by QSY7. Cy3 emission at 580 nm was recovered upon MMP2-responsive Pep-QSY7 cleavage. Epidermal growth factor antibody (Anti-EGFR) was then conjugated to UCNPs *via* a PEG_{44} linker for the specific anchoring of upconversion nanoprobe UCNPs-Cy3/Pep-QSY7/Ab to EGFR on the tumor cell membrane (Scheme 1A). MMP2 encountered the cell membrane-anchored upconversion nanoprobe UCNPs-Cy3/Pep-QSY7/Ab immediately after secretion and was confined in the extracellular local area, which resulted in fast and sensitive Cy3 luminescence recovery at 580 nm under 980 nm irradiation. Another emission of UCNPs at 654 nm remained unchanged during the peptide cleavage process, which acted as an internal standard for quantitative imaging Cy3 secretion *in situ* (Scheme 1B). The as-prepared cell membrane-anchored protease secretion monitoring system was successively applied for *in vivo* MMP imaging from metastatic lymph nodes and would have promising applications in cancer diagnosis and therapy.

EXPERIMENTAL SECTION

Synthesis of UCNPs $NaYF_4$:Gd,Yb,Er@$NaYF_4$. YCl_3 (0.70 mmol), $YbCl_3$ (0.18 mmol), $GdCl_3$ (0.10 mmol), and $ErCl_3$ (0.02 mmol) were mixed with 5 mL of OA and 15 mL of ODE, heated to 150 °C, and stirred for 60 min under vacuum. After the reaction solution was cooled down to 45 °C, 10 mL of methanol containing NH_4F (4.00 mmol) and NaOH (2.50 mmol) was added dropwise and continuously stirred for 30 min. After heating at 110 °C for 15 min to completely remove methanol, the mixture was heated to 300 °C and kept for 90 min under nitrogen to get the core of UCNPs $NaYF_4$:Gd,Yb,Er. The UCNPs shell precursor $NaYF_4$ was prepared in the same way above and added into the above prepared UCNPs core $NaYF_4$:Gd,Yb,Er, and the reaction mixture was stirred for another 30 min at 300 °C and cooled down to room temperature. The as-obtained UCNPs $NaYF_4$:Gd,Yb,Er@$NaYF_4$ with a core−shell structure was precipitated with 20 mL of acetone and redispersed in 5 mL of cyclohexane.

Preparation of Upconversion Nanoprobe (UCNPs-Cy3/Pep-QSY7/Ab). The above-prepared UCNPs (200 mg) was dispersed in $CHCl_3$ (10 mL) and mixed with EtOH (4 mL)/water (6 mL, pH adjusted to 2−3 with 1 M HCl)

https://doi.org/10.1021/acs.analchem.1c00469
Anal. Chem. 2021, 93, 7258−7265

solution. Alendronic acid (ADA) (50 mg) was then added in the above solution for UCNPs surface functionalization with amine group and increasing their water dispersity. After stirring at 880 rpm for 30 min at room temperature, the as-obtained UCNPs-ADA in the upper aqueous solution was collected and washed with water thrice.

To prepare upconversion nanoprobe UCNPs-Cy3/Pep-QSY7/Ab, UCNPs-ADA (1 mg/mL) was mixed with different concentrations of NHS-Cy3 (10, 20, 30, and 40 μM), NHS-PEG_2-Mal (240 μM), and NHS-PEG_{44}-NHS (30 μM) in DMF (300 μL). The reaction mixture was stirred overnight at 37 °C and washed with DMF thrice to get a series of UCNPs-Cy3/PEG_2/PEG_{44} with various amounts of surface-modified Cy3. The fluorescence intensities of Cy3 at 580 nm from the as-obtained UCNPs-Cy3/PEG_2/PEG_{44} were compared to determine the optimal reaction concentration of NHS-Cy3 as 30 μM. UCNPs-Cy3/PEG_2/PEG_{44} (1 mg/mL) with the optimal surface amount of Cy3 was then mixed with various concentrations of Pep-QSY7 (2, 3, 4, and 5 μM) in 300 μL of DMF, stirred overnight, and washed with DMF thrice. Cy3 fluorescence intensities at 580 nm were measured again to determine the optimal reaction concentration of Pep-QSY7 as 5 μM for complete quenching of Cy3 emission. Anti-EGFR (5 μL, 0.3 mg/mL) was then added into the above-prepared UCNPs-Cy3/Pep-QSY7/PEG_{44}, and the reaction mixture was placed on a shaking plate at 37 °C for 2 h. The resulting solution was then centrifuged at 2500 rcf for 20 min and washed with PBS to get the upconversion nanoprobe UCNPs-Cy3/Pep-QSY7/Ab. The amount of modified ADA on the nanoprobe was quantified by titrating with ninhydrin, and the amounts of modified Cy3, Pep-QSY7, on the nanoprobe were quantified by measuring the characteristic absorbance peak at 564 nm.

Detection of Cell-Secreted MMP2. MDA-MB-231 cells were seeded in four-well confocal dishes and incubated at 37 °C for 24 h. To suppress spontaneous MMP2 secretion as a background signal, cells were treated with an MMP2 activity inhibitor 1,10-phenanthroline (50 μg/mL) for 1 h. To couple upconversion nanoprobe to the cell membrane, the cells were subsequently incubated with fresh RPMI-1640 media containing UCNPs-Cy3/Pep-QSY7/Ab (0.1 mg/mL) and 1,10-phenanthroline (50 μg/mL) for another 1 h. To evaluate the MMP2 sensing capability of cell surface anchoring upconversion nanoprobe UCNPs-Cy3/Pep-QSY7/Ab, enzyme kinetic studies were conducted. Cells were fixed in 4% paraformaldehyde at room temperature for 10 min after removing unbound upconversion nanoprobes by washing with PBS thrice and then washed by PBS thrice. Different concentrations of MMP2 (5, 10, 20, 40, and 80 ng/mL) were added to initiate the reactions. The CLSM fluorescence images under 980 nm excitation were recorded at various time points. For cell-secreted MMP2 monitoring, the cells were incubated with fresh RPMI-1640 media containing LPS (50 μg/mL) to stimulate MMP2 secretion, and the cell-secreted MMP2 was monitored for 1 h *via* CLSM fluorescence images under 980 nm excitation. Cy3 luminescence recovery at 550−600 nm was collected as an MMP2 secretion signal, and the UCNPs characteristic signal at 630−680 nm was collected as an internal standard. MMP secretion from MCF-7 cells was also imaged according to the same procedure mentioned above. To demonstrate the superiority of cell membrane-anchored probes in cell secretion monitoring, MDA-MB-231 cells were also incubated with the Anti-EGFR free upconversion nanoprobe UCNPs-Cy3/Pep-QSY7, and the corresponding Cy3 luminescence recovery and UCNPs characteristic luminescence were measured, respectively, from cell culture media.

***In Vivo* MMP Imaging on Mice Tumor.** Female BALB/c nude mice (5−6 weeks) were purchased from Keygen Biotech (Nanjing, China). All animal experiments were approved by the Model Animal Research Center of Nanjing University (MARC) and followed the institutional animal use and care regulations. 1×10^6 MDA-MB-231 cells were injected subcutaneously into the left hind foot sole of each mouse, and the metastatic tumor was established when the left popliteal fossa lymph node swelled up. For *in vivo* imaging, 25 μL of UCNPs-Cy3/Pep-QSY7/Ab (0.1 mg/mL) was injected subcutaneously into the middle site of the left leg, and the Cy3 luminescence recovery was imaged at various time points just before injection and 0.5, 1, 2, and 4 h after injection. The BALB/c nude mice in the absence of metastasis tumor model were served as a control group and treated with the same procedure.

To verify the responsiveness of nanoprobes to MMP2 *in vivo*, the MMP2 inhibitor 1,10-phenanthroline (25 μL, 50 μg/mL) was injected into metastatic tumors 1 h before subcutaneous injection of nanoprobes, followed by the procedure above. All experiments were conducted respectively in three mice. The corresponding fluorescence intensities were quantified by the ROIs measurement using Living Image Software.

RESULTS AND DISCUSSION

Construction of Upconversion Nanoprobe UCNPs-Cy3/Pep-QSY7/Ab. Core−shell structured UCNPs ($NaYF_4$:Gd,Yb,Er@$NaYF_4$) with 10% of Gd^{3+}, 18% of Yb^{3+}, and 2% of Er^{3+} were synthesized according to our previously reported method.[35] UCNPs core $NaYF_4$:Gd,Yb,Er showed a uniform size of 22.8 ± 1.1 nm (Figure 1A) and emission peaks corresponding to $^2H_{11/2} \rightarrow {}^4I_{15/2}$, $^4S_{3/2} \rightarrow {}^4I_{15/2}$, $^4F_{9/2} \rightarrow {}^4I_{15/2}$ transitions of Er^{3+} at 520, 540, and 654 nm, respectively, upon 980 nm excitation (Figure S1). The coating of the $NaYF_4$ shell increased the particle size to 24.4 ± 1.3 nm (Figure 1B) and dramatically increased UCNPs luminescence due to the prevention from surface quenching (Figure S1). UCNPs surface ligand OA was then exchanged with bidentate ligand ADA with an amine terminus group, which increased particle water dispersity and facilitated further functionalization. The successful ligand exchange was confirmed by Fourier transform infrared (FT-IR) spectra, which demonstrated the appearance of ADA characteristic absorption peak at 1160 cm^{-1} corresponding to P═O stretching vibration for ADA-functionalized UCNPs (UCNPs-ADA), accompanying with the disappearance of OA characteristic absorption peak at 2920 cm^{-1} corresponding to $-CH_2-$ stretching vibration (Figure 1C, lines 1 and 2). The as-prepared UCNPs-ADA has a hydrodynamic diameter of 32.4 ± 2.3 nm and a zeta potential of 37.2 ± 1.5 mV (Figure 1D, UCNPs-ADA). The stoichiometry of ADA on UCNPs-ADA surface was quantified by titrating with ninhydrin, which reacts with amino group and produces a blue-purple compound, and 5346 ± 211 ADA per UCNPs was determined by comparing with the ninhydrin standard calibration curve (Figure S2A−C).

Dye Cy3 was subsequently conjugated to the UCNPs-ADA *via* amide bond. The characteristic absorption band of Cy3 appears in the range of 500−600 nm, which well overlapped with the emission peak of UCNPs at 540 nm (Figure 1E, lines

https://doi.org/10.1021/acs.analchem.1c00469
Anal. Chem. 2021, 93, 7258−7265

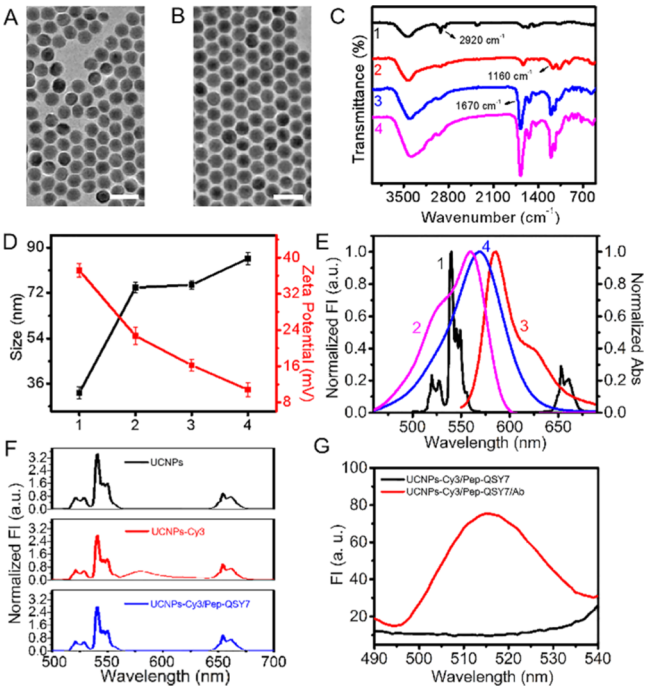

Figure 1. TEM images of (A) $NaYF_4$:Gd,Yb,Er and (B) UCNPs. The scale bar in A, B is 50 nm. (C) FT-IR spectra of (1) UCNPs, (2) UCNPs-ADA, (3) UCNPs-Cy3/Pep-QSY7, and (4) UCNPs-Cy3/Pep-QSY7/Ab. (D) Zeta potential and hydrodynamic sizes of (1) UCNPs-ADA, (2) UCNPs-Cy3/PEG_2/PEG_{44}, (3) UCNPs-Cy3/Pep-QSY7, and (4) UCNPs-Cy3/Pep-QSY7/Ab. (E) Upconversion luminescence spectrum of UCNPs (line 1), fluorescence spectrum of Cy3 (line 3), UV−Vis absorption spectra of Cy3 (line 2), and QSY7 (line 4). (F) UCL spectra of UCNPs, UCNPs-Cy3, and UCNPs-Cy3/Pep-QSY7. (G) Fluorescence spectra of UCNPs-Cy3/Pep-QSY7 and UCNPs-Cy3/Pep-QSY7/Ab incubated with FITC-labeled secondary Anti-EGFR.

1 and 2). The as-obtained UCNPs-Cy3 demonstrated strong Cy3 emission at 580 nm upon 980 nm excitation with the suppression of UCNPs emission at 540 nm due to the resonance energy transfer process (Figure 1F, UCNPs-Cy3). NHS-PEG_2-Mal and NHS-PEG_{44}-NHS were also conjugated to UCNP surface for the subsequent linking of Pep-QSY7 and Anti-EGFR, which increased the hydrodynamic diameter to 74.1 ± 2.0 nm and decreased the zeta potential to 22.7 ± 1.9 mV (Figure 1D, UCNPs-Cy3/PEG_2/PEG_{44}). The as-prepared UCNPs-Cy3/PEG_2/PEG_{44} was subsequently functionalized with QSY7-labeled MMP2-specific substrate peptide GPLGVRGC (Pep-QSY7), and the successful conjugation was confirmed by the appearance of −CONH− characteristic peak at 1670 cm^{-1} in the FT-IR spectrum (Figure 1C, line 3). The absorption of QSY7 in the range of 550−650 nm matches well with the emission peak of Cy3 at 580 nm (Figure 1E, lines 3 and 4), which resulted in the continuous resonance energy transfer from Cy3 to QSY7 with the complete suppression of Cy3 emission peak at 580 nm (Figure 1F, UCNPs-Cy3/Pep-QSY7). Luminescence lifetime was also measured to confirm the continuous resonance energy transfer process. The modification of Cy3 decreased the luminescence lifetime of UNCPs at 540 nm from 105 to 70 μs (Figure S3A), which was remained at 70 μs after the subsequent conjugation of Pep-QSY7, indicating that the continuous energy transfer process did not affect energy transfer efficiency from UCNPs to Cy3. There was no direct energy transfer from UCNPs emission at 540 nm to QSY7 at the peptide terminus, and the 540 nm emission of UCNPs-Pep-QSY7 kept the same intensity and lifetime as that of UCNPs (Figure S3B,C). The lifetime for UCNPs emission at 654 nm remained at 258 μs for UCNPs, UCNPs-Cy3, and UCNPs-Cy3/Pep-QSY7 (Figure S3D). The incubation concentrations of Cy3 and Pep-QSY7 in the surface modification process were further optimized, and the maximum Cy3 luminescence intensity at 580 nm was obtained at 30 μM Cy3 (Figure S4A), while 5 μM Pep-QSY7 could completely suppress the Cy3 luminescence (Figure S4B). The amounts of Cy3 and Pep-QSY7 per UCNPs were further quantified by measuring their characteristic absorbance at 564 nm and compared with Cy3/QSY7 respective standard calibration curves, which resulted in 143 ± 2 Cy3 per UCNPs for UCNPs-Cy3 (Figure S2D−F) and 39 ± 3 Pep-QSY7 per UCNPs for UCNPs-Cy3/Pep-QSY7 (Figure S2G−I).

To anchor the upconversion nanoprobe to tumor cells, Anti-EGFR, which specifically targets the tumor cell membrane-overexpressed protein EGFR, was conjugated to nanoparticle surface *via* NHS-PEG_{44}-NHS linker to complete the upconversion nanoprobe UCNPs-Cy3/Pep-QSY7/Ab. The as-prepared UCNPs-Cy3/Pep-QSY7/Ab continuously decreased the zeta potential to 10.8 ± 1.5 mV and increased the hydrodynamic diameter to 85.7 ± 2.3 nm (Figure 1D). The successful surface functionalization of Anti-EGFR was further confirmed by incubating UCNPs-Cy3/Pep-QSY7/Ab with FITC-labeled secondary Anti-EGFR, which demonstrated obvious FITC fluorescence at 515 nm (Figure 1G, red line). On the contrary, UCNPs-Cy3/Pep-QSY7 barely demonstrated fluorescence at 515 nm after incubating with FITC-labeled secondary Anti-EGFR (Figure 1G, black line).

***In Vitro* Response of Upconversion Nanoprobe UCNPs-Cy3/Pep-QSY7/Ab to MMP2.** The MMP2-responsive peptide cleavage and the corresponding QSY7 release disrupted LRET between Cy3 and QSY7 on the upconversion nanoprobe and resulted in the gradual luminescence recovery of Cy3 at 580 nm under 980 nm irradiation according to the MMP2 concentration (Figure 2A). The continuous Cy3 luminescence recovery did not affect UCNPs another emission at 654 nm, which retained the same intensity in response to different MMP2 concentrations (Figure 2A). Therefore, UCNPs luminescence at 654 nm was taken as the internal standard for MMP2 detection, and the intensity of Cy3 luminescence recovery was corrected by comparing with the intensity of the internal standard (FI580/FI654). The luminescence ratio of FI580/FI654 gradually increased according to the MMP2 concentration and demonstrated a linear range from 1 to 100 ng/mL with the limit of detection as 0.51 ng/mL (Figure 2B). The detection sensitivity was comparable to the previously reported MMP2 detection probes that applied for MMP2 detection in a homogeneous solution[11,36] or MMP2 secretion detection in cell supernatants,[37,38] guaranteeing its application for *in situ* MMP2 secretion monitoring.

To demonstrate the reaction specificity of upconversion nanoprobe to MMP2, it was treated with 500 ng/mL of nonspecific protease such as caspase3, MMP1, MMP9, and 50 ng/mL of MMP2 in the presence of its inhibitor 1,10-phenanthroline, respectively. Besides, the nonspecific upconversion nanoprobe UCNPs-Cy3/nsPep-QSY7/Ab was also incubated with 50 ng/mL of MMP2 to confirm the specific cleavage of peptide. All results showed negligible response

https://doi.org/10.1021/acs.analchem.1c00469
Anal. Chem. 2021, 93, 7258−7265

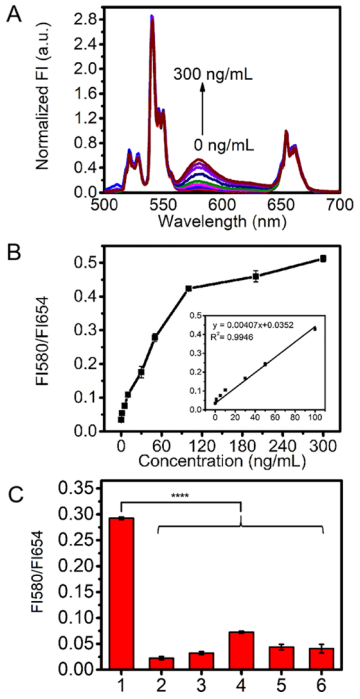

Figure 2. (A) Upconversion emission spectra of UCNPs-Cy3/Pep-QSY7/Ab in response to different concentrations of MMP2 and (B) corresponding linear relationship of FI580/FI654 against MMP2 concentration. (C) Luminescence intensity ratio FI580/FI654 of UCNPs-Cy3/Pep-QSY7/Ab incubated with (1) 50 ng/mL MMP2, 500 ng/mL (2) caspase3, (3) MMP1, (4) MMP9, (5) 50 ng/mL MMP2 with inhibitor, and (6) UCNPs-Cy3/nsPep-QSY7/Ab incubated with 50 ng/mL MMP2. The error bars indicate means and S.D. (n = 3). ****P < 0.0001 with two-tailed Student's t-test.

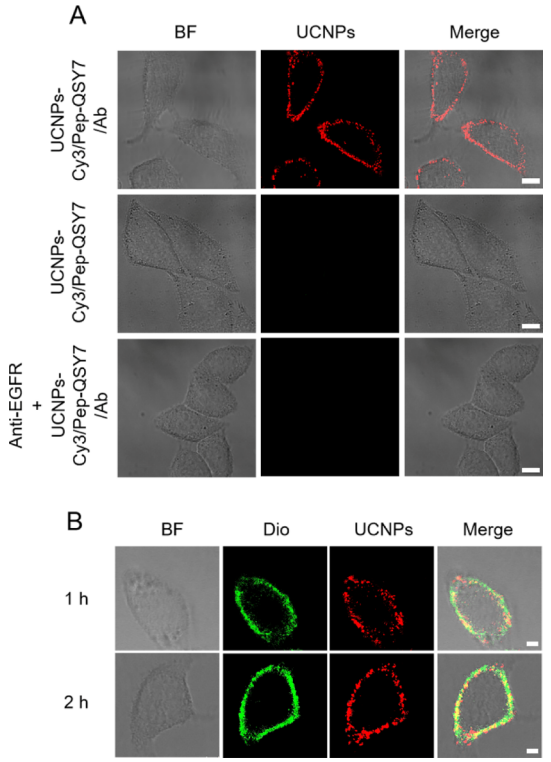

Figure 3. Confocal microscopy images of (A) MDA-MB-231 cells incubated with UCNPs-Cy3/Pep-QSY7/Ab, UCNPs-Cy3/Pep-QSY7, and excess Anti-EGFR + UCNPs-Cy3/Pep-QSY7/Ab. The scale bar is 10 μm. (B) Upconversion nanoprobes (UCNPs) and MDA-MB-231 cell membrane (Dio) after 1 and 2 h of incubation. The scale bar is 5 μm.

compared with the response of the upconversion nanoprobe UCNPs-Cy3/Pep-QSY7/Ab to 50 ng/mL of MMP2 (Figure 2C), indicating good reaction specificity of the upconversion nanoprobe.

The serum stability of the upconversion nanoprobe was evaluated by monitoring the Cy3 luminescence recovery in PBS and RPMI-1640 cell culture media containing 10% fetal bovine serum (FBS) for 12 h. Neither of them showed an obvious increase for Cy3 luminescence intensity (Figure S5). Besides, the upconversion nanoprobe also retained the stable hydrodynamic size (Figure S6A) and polymer dispersity index (PDI) (Figure S6B) during 12 h incubation in PBS and RPMI-1640 media containing 10% FBS. These results indicated the capability of the as-prepared upconversion nanoprobe for *in vivo* imaging.

Anchoring of Upconversion Nanoprobe to the Cell Membrane. MDA-MB-231 cells, which exhibit high MMP activities along with metastatic tendency,[39] was chosen as the sample cell for *in situ* MMP2 secretion monitoring. The upconversion nanoprobe UCNPs-Cy3/Pep-QSY7/Ab incubated MDA-MB-231 cells showed clear UCNPs luminescence from cell membrane (Figure 3A, UCNPs-Cy3/Pep-QSY7/Ab), indicating the efficient anchoring of the upconversion nanoprobe.

To show the binding positions of the upconversion nanoprobe, it was colocalized with the cell membrane under CLSM. After 1 h of incubation, UCNPs luminescence at 654 nm was completely overlapped with cell membrane labeling dye Dio luminescence at 501 nm (Figure 3B, 1 h), indicating the efficient anchoring of upconversion nanoprobe on the cell membrane. EGFR remained stable at the cell membrane,[40] and UCNPs luminescence at 654 nm still overlapped well with that of dye Dio after 2 h of incubation (Figure 3B, 2 h), indicating that the upconversion nanoprobes were not uptaken into cells during the period of *in situ* MMP secretion detection process. The Z-stack images also revealed little UCNPs luminescence from cellular interior (Figure S7), confirming the stable location of the upconversion nanoprobe on the cell membrane. To verify the anchoring specificity of the upconversion nanoprobe to tumor cell membrane, a series of control experiments were performed. MDA-MB-231 cells incubated with Anti-EGFR free upconversion nanoprobe UCNPs-Cy3/Pep-QSY7 barely showed UCNPs luminescence on the cell membrane (Figure 3A, UCNPs-Cy3/Pep-QSY7). The cell surface anchoring of the upconversion nanoprobe was also prevented for excess Anti-EGFR pre-treated MDA-MB-231 cells (Figure 3A, Anti-EGFR + UCNPs-Cy3/Pep-QSY7/Ab).

The cytotoxicity of the upconversion nanoprobe was then verified by the MTT assay. The cell viability of the upconversion nanoprobe-anchored MDA-MB-231 cells was compared with that of unmodified MDA-MB-231 cells, and both reached 95% of cell viability (Figure S8A). Flow cytometry analysis barely showed differences in cell morphology (Figure S8B) and viability (Figure S8C) for upconversion nanoprobe-anchored MDA-MB-231 cells, revealing the low cytotoxicity of the upconversion nanoprobe.

***In Situ* Monitoring of MMP2 Secretion from Cells.** MMP2-sensing capability of cell surface anchoring upconversion nanoprobe was first evaluated by challenging it with

https://doi.org/10.1021/acs.analchem.1c00469
Anal. Chem. 2021, 93, 7258−7265

recombinant MMP2. Upconversion nanoprobe-anchored MDA-MB-231 cells were immobilized on the substrate and incubated with different concentrations of recombinant MMP2. The ratio of Cy3 fluorescence recovery at 580 nm over internal luminescence intensity at 654 nm (FI580/FI654) showed a typical time-resolved increase in 50 min for all MMP2 concentrations (Figure S9A). The kinetic parameter k_{cat} and Michaelis constant (K_m) were determined to be 1.333 min^{-1} and 166.7 nM from the Lineweaver−Burk plot (Figure S9B). The ratio k_{cat}/K_m was calculated to be 1.3×10^5 M^{-1} s^{-1}, which was comparable to the previously reported values,[41,42] confirming an efficient MMP2 enzymatic cleavage toward cell membrane-anchored upconversion nanoprobe.

To *in situ* monitor MMP2 secretion, upconversion nanoprobe-anchored MDA-MB-231 cells were activated by LPS, and the luminescence recovery of Cy3 at 580 nm upon 980 nm irradiation in accordance with upconversion luminescence at 654 nm were measured for 1 h. Cy3 luminescence on the cell membrane demonstrated time-dependent intensity increase due to the continuous secretion of MMP2 and cascade cleavage of QSY7 from the upconversion nanoprobe (Figure 4A), while the intensity for internal luminescence at 654 nm remained the same during the measurement process (Figure S10). The luminescence intensity ratio of FI580/FI654 was plotted over time and showed a steep increase immediately post-LPS activation. The signal increase saturated at 50 min while FI580/FI654 reached 0.48 (Figure 4B, red line, Figure S11A, column 1), which was comparable to the saturation value of the solution-dispersed upconversion nanoprobe for *in vitro* MMP2 measurement (Figure 2B), indicating the high reaction efficiency of cell membrane-anchored upconversion nanoprobe and the complete cleavage of the substrate peptide in the cell membrane-anchored upconversion nanoprobe. In comparison, the upconversion nanoprobes UCNPs-Cy3/Pep-QSY7 in the absence of Anti-EGFR labeling were incubated with the same amount of MDA-MB-231 cells, and the supernatant was collected at different time points post-LPS activation up to 2 h for fluorescence spectrum measurements (Figure 4C). Similar to the cell membrane-anchored upconversion nanoprobe, the supernatant-dispersed nanoprobe UCNPs-Cy3/Pep-QSY7 also demonstrated time-dependent Cy3 fluorescence recovery (Figure 4B, black line). Unlike the steep signal increase immediately post-LPS activation for cell membrane-anchored nanoprobe, the supernatant-dispersed upconversion nanoprobe demonstrated a much milder signal increase in the beginning period, indicating the diffusion-controlled reaction process.[43] Cell-secreted MMP2 needs to migrate longer distance to react with the solution-dispersed probe UCNPs-Cy3/Pep-QSY7, which impaired reaction efficiency compared with the cell membrane-anchored nanoprobe.

The upconversion nanoprobes were further anchored to MCF-7 cells, which have a similar expression level of EGFR on the cell membrane and lower secretion of MMP2.[44] The fluorescence recovery of Cy3 from MCF-7 cell membrane was less strong compared with that from MDA-MB-231 cells (Figure 4D, MCF-7), and the fluorescence ratio of FI580/FI654 was calculated as 0.22 at 50 min post-LPS activation (Figure S11A, column 2). In addition, MDA-MB-231 cells were treated with the MMP2 inhibitor 1,10-phenanthroline to suppress its activities and set as the negative control. The suppression of MMP2 activities did not affect surface anchoring of the upconversion nanoprobe and still demonstrated stable UCNPs 654 nm luminescence on the membrane of MDA-MB-231 cells, while Cy3 fluorescence recovery was barely observed due to the deactivation of MMP2 (Figure 4D, inhibitor) with FI580/FI654 of 0.06 (Figure S11A, column 3). Supernatant-dispersed upconversion nanoprobe UCNPs-Cy3/Pep-QSY7 also demonstrated a similar tendency of FI580/FI654 values as membrane-anchored nanoprobes for MDA-MB-231 cells, MCF-7 cells, and inhibitor-treated MDA-MB-231 cells (Figure S11B), indicating the accuracy of cell membrane-anchored nanoprobe for monitoring MMP2 secretion.

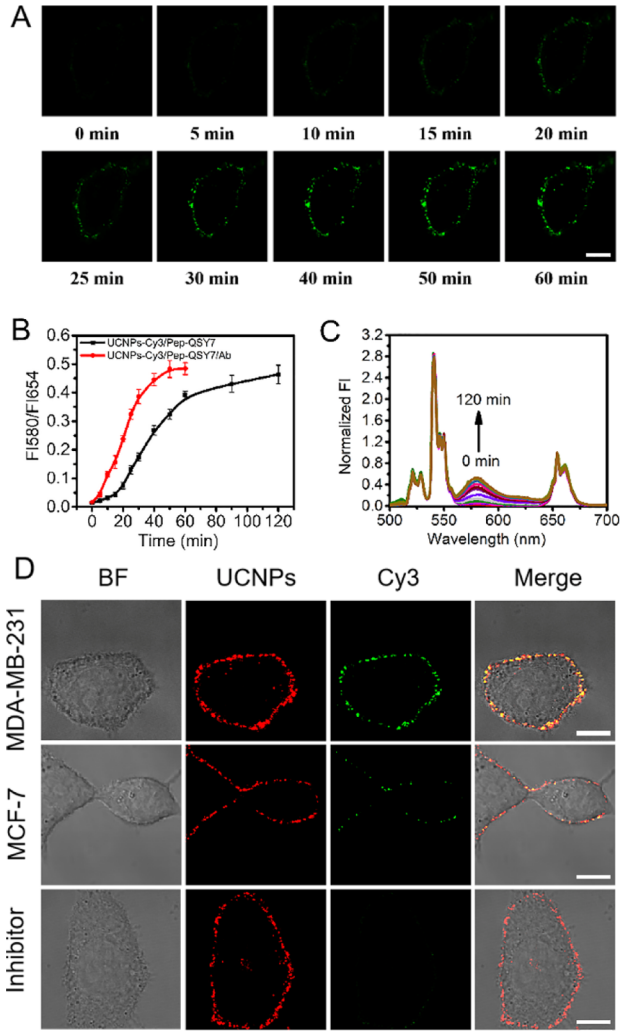

Figure 4. (A) Time-dependent imaging of Cy3 luminescence upon NIR irradiation from the upconversion nanoprobe-anchored MDA-MB-231 cell membrane. (B) FI580/FI654 in response to MMP2 secretion according to time for the upconversion nanoprobe anchored on MDA-MB-231 cell membrane (UCNPs-Cy3/Pep-QSY7/Ab) and dispersed in the supernatant (UCNPs-Cy3/Pep-QSY7) and (C) corresponding UCL spectra of supernatant-dispersed UCNPs-Cy3/Pep-QSY7. (D) Confocal microscopy images of upconversion nanoprobe-anchored MDA-MB-231 cells, MCF-7 cells, and inhibitor pre-treated MDA-MB-231 cells upon LPS activation. The scale bar is 10 μm.

Imaging of Metastatic Lymph Node *In Vivo*. Considering the close relationship between MMP secretion and tumor metastasis, the *in vivo* MMP imaging was used for the imaging of metastatic lymph node.[3,4,45] The metastatic lymph node of breast tumor was established as a metastatic tumor model due

https://doi.org/10.1021/acs.analchem.1c00469
Anal. Chem. 2021, 93, 7258−7265

to the high risk of breast cancer for metastasis.[46] The capability of cell membrane-anchored upconversion nanoprobe for metastasis imaging was confirmed by *in vivo* measuring Cy3 luminescence recovery.

The metastatic lymph node demonstrated continued increased Cy3 fluorescence until it reached plateau 1 h post-injection. In comparison, the normal lymph node did not display Cy3 fluorescence under the same experimental condition. This result was expected since the metastatic lymph node is more invasive accompanying with higher tendency of protease secretion.[44,47] To demonstrate the reaction specificity to MMP2, 1,10-phenanthroline was also used to treat the metastatic lymph node to suppress the MMP2 activity, which barely showed Cy3 fluorescence recovery post *in vivo* injection (Figure 5). These results demonstrated the applicability of upconversion nanoprobe for *in vivo* protease secretion imaging and would potentially contribute to the assessment of tumor invasiveness and metastatic potential.

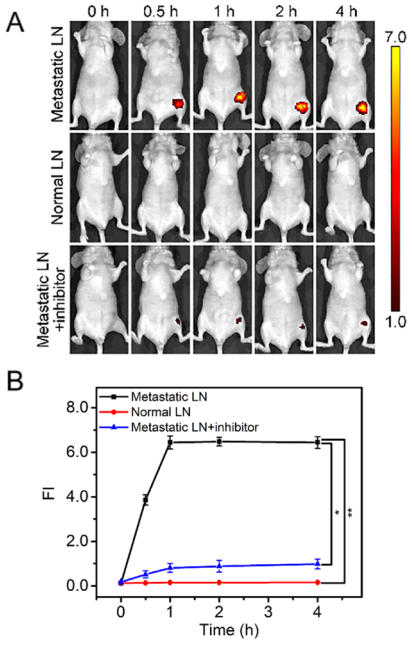

Figure 5. (A) Fluorescence images and (B) average fluorescence intensities of Cy3 at 580 nm from metastatic lymph node, normal lymph node, and metastatic lymph node with the inhibitor in living mice before (0 h) and 0.5, 1, 2, and 4 h post UCNPs-Cy3/Pep-QSY7/Ab injection. *P < 0.05 and **P < 0.01 with two-tailed Student's t-test.

CONCLUSIONS

In summary, a tumor membrane-anchored ratiometric upconversion nanoprobe was constructed for *in situ* protease secretion monitoring. The luminescence of Cy3 in the upconversion nanoprobe was recovered in response to MMP2 secretion, while the other emission of UCNPs at 654 nm was used as an internal standard to achieve ratiometric imaging. Anti-EGFR functionalization of the nanoprobe located it in the vicinity of the tumor cell membrane to achieve efficient response of MMP2 secretion. *In situ* monitoring of MMP2 secretion was achieved from MDA-MB-231 cells and MCF-7 cells with successful application for *in vivo* metastatic lymph nodes imaging. Thus, we believe that the presented strategy of *in situ* monitoring MMP2 secretion would be easily extended to other analytes and provide a powerful platform for cellular secretion study and tumor metastasis assessment.

ASSOCIATED CONTENT

Supporting Information

The Supporting Information is available free of charge at https://pubs.acs.org/doi/10.1021/acs.analchem.1c00469.

Materials and reagents, apparatus, *in vitro* detection of MMP2, serum stability and colloidal stability of UCNPs-Cy3/Pep-QSY7/Ab, cellular surface anchoring of UCNPs-Cy3/Pep-QSY7/Ab, and cytotoxicity of UCNPs-Cy3/Pep-QSY7/Ab (PDF)

AUTHOR INFORMATION

Corresponding Author

Ying Liu − *State Key Laboratory of Analytical Chemistry for Life Science, School of Chemistry and Chemical Engineering, Nanjing University, Nanjing 210023, China; Chemistry and Biomedicine Innovation Center, Nanjing University, Nanjing 210023, China;* orcid.org/0000-0001-5718-7804; Phone: +86-(0)25-89681918; Email: yingliu@nju.edu.cn

Authors

Yanyun Fang − *State Key Laboratory of Analytical Chemistry for Life Science, School of Chemistry and Chemical Engineering, Nanjing University, Nanjing 210023, China*

Yuetong Li − *State Key Laboratory of Analytical Chemistry for Life Science, School of Chemistry and Chemical Engineering, Nanjing University, Nanjing 210023, China*

Yuyi Li − *State Key Laboratory of Analytical Chemistry for Life Science, School of Chemistry and Chemical Engineering, Nanjing University, Nanjing 210023, China*

Rong He − *State Key Laboratory of Analytical Chemistry for Life Science, School of Chemistry and Chemical Engineering, Nanjing University, Nanjing 210023, China*

Yue Zhang − *State Key Laboratory of Analytical Chemistry for Life Science, School of Chemistry and Chemical Engineering, Nanjing University, Nanjing 210023, China; School of Pharmacy, Nanjing University of Chinese Medicine, Nanjing 210023, China;* orcid.org/0000-0002-7902-4253

Xiaobo Zhang − *State Key Laboratory of Analytical Chemistry for Life Science, School of Chemistry and Chemical Engineering, Nanjing University, Nanjing 210023, China;* orcid.org/0000-0003-0222-2515

Huangxian Ju − *State Key Laboratory of Analytical Chemistry for Life Science, School of Chemistry and Chemical Engineering, Nanjing University, Nanjing 210023, China;* orcid.org/0000-0002-6741-5302

Complete contact information is available at: https://pubs.acs.org/10.1021/acs.analchem.1c00469

Notes

The authors declare no competing financial interest.

ACKNOWLEDGMENTS

We gratefully acknowledge the National Natural Science Foundation of China (21974064, 22022405, and 21635005), the Natural Science Foundation of Jiangsu Province for distinguished Young Scholars (BK20200010), the Specially-appointed Professor Foundation of Jiangsu Province, Program for Innovative Talents and Entrepreneurs of Jiangsu Province,

State Key Laboratory of Analytical Chemistry for Life Science (5431ZZXM2003), and the Fundamental Research Funds for the central universities (14380472).

REFERENCES

(1) Wolf, K.; Wu, Y. I.; Liu, Y.; Geiger, J.; Tam, E.; Overall, C.; Stack, M. S.; Friedl, P. *Nat. Cell Biol.* **2007**, *9*, 893−904.
(2) Egeblad, M.; Werb, Z. *Nat. Rev. Cancer* **2002**, *2*, 161−174.
(3) Savariar, E. N.; Felsen, C. N.; Nashi, N.; Jiang, T.; Ellies, L. G.; Steinbach, P.; Tsien, R. Y.; Nguyen, Q. T. *Cancer Res.* **2013**, *73*, 855−864.
(4) Yin, L.; Sun, H.; Zhao, M.; Wang, A.; Qiu, S.; Gao, Y.; Ding, J.; Ji, S.-J.; Shi, H.; Gao, M. *J. Org. Chem.* **2019**, *84*, 6126−6133.
(5) Kessenbrock, K.; Plaks, V.; Werb, Z. *Cell* **2010**, *141*, 52−67.
(6) Liotta, L. *Cancer Res.* **1986**, *46*, 1−7.
(7) Stadnik, T. W.; Chaskis, C.; Michotte, A.; Shabana, W. M.; van Rompaey, K.; Luypaert, R.; Budinsky, L.; Jellus, V.; Osteaux, M. *Am. J. Neuroradiol.* **2001**, *22*, 969−976.
(8) Nakanishi, K.; Kobayashi, M.; Nakaguchi, K.; Kyakuno, M.; Hashimoto, N.; Onishi, H.; Maeda, N.; Nakata, S.; Kuwabara, M.; Murakami, T.; Nakamura, H. *Magn. Reson. Med. Sci.* **2007**, *6*, 147−155.
(9) Smith, E. H. *Rev. Radiol.* **1991**, *178*, 253−258.
(10) Mankin, H. J.; Mankin, C. J.; Simon, M. A. *J. Bone Jt. Surg., Am. Vol.* **1996**, *78*, 656−663.
(11) Cheng, H.; Li, S.-Y.; Zheng, H.-R.; Li, C.-X.; Xie, B.-R.; Chen, K.-W.; Li, B.; Zhang, X.-Z. *Anal. Chem.* **2017**, *89*, 4349−4354.
(12) Gao, X.; Jiang, L.; Hu, B.; Kong, F.; Liu, X.; Xu, K.; Tang, B. *Anal. Chem.* **2018**, *90*, 4719−4724.
(13) Zhang, X.; Miao, Z.; Hu, Y.; Yang, X.; Tang, Y.; Zhu, D. *Sens. Actuators, B* **2018**, *273*, 511−518.
(14) Chen, C.-H.; Sarkar, A.; Song, Y.-A.; Miller, M. A.; Kim, S. J.; Griffith, L. G.; Lauffenburger, D. A.; Han, J. *J. Am. Chem. Soc.* **2011**, *133*, 10368−10371.
(15) Wang, Y.; Shen, P.; Li, C.; Wang, Y.; Liu, Z. *Anal. Chem.* **2012**, *84*, 1466−1473.
(16) Fan, G.-C.; Han, L.; Zhu, H.; Zhang, J.-R.; Zhu, J.-J. *Anal. Chem.* **2014**, *86*, 12398−12405.
(17) Nie, Y.; Zhang, P.; Wang, H.; Zhuo, Y.; Chai, Y.; Yuan, R. *Anal. Chem.* **2017**, *89*, 12821−12827.
(18) Xu, S.; Liu, H.-W.; Yin, X.; Yuan, L.; Huan, S.-Y.; Zhang, X.-B. *Chem. Sci.* **2019**, *10*, 320−325.
(19) Mu, J.; Liu, F.; Rajab, M. S.; Shi, M.; Li, S.; Goh, C.; Lu, L.; Xu, Q.-H.; Liu, B.; Ng, L. G.; Xing, B. *Angew. Chem., Int. Ed.* **2014**, *53*, 14357−14362.
(20) Orynbayeva, Z.; Kolusheva, S.; Livneh, E.; Lichtenshtein, A.; Nathan, I.; Jelinek, R. *Angew. Chem., Int. Ed.* **2005**, *44*, 1092−1096.
(21) Zhao, W.; Schafer, S.; Choi, J.; Yamanaka, Y. J.; Lombardi, M. L.; Bose, S.; Carlson, A. L.; Phillips, J. A.; Teo, W.; Droujinine, I. A.; Cui, C. H.; Jain, R. K.; Lammerding, J.; Love, J. C.; Lin, C. P.; Sarkar, D.; Karnik, R.; Karp, J. M. *Nat. Nanotechnol.* **2011**, *6*, 524−531.
(22) You, M.; Lyu, Y.; Han, D.; Qiu, L.; Liu, Q.; Chen, T.; Sam Wu, C.; Peng, L.; Zhang, L.; Bao, G.; Tan, W. *Nat. Nanotechnol.* **2017**, *12*, 453−459.
(23) Gao, T.; Chen, T.; Feng, C.; He, X.; Mu, C.; Anzai, J.-i.; Li, G. *Nat. Commun.* **2019**, *10*, 2946.
(24) Gao, T.; Wang, B.; Shi, L.; Zhu, X.; Xiang, Y.; Anzai, J.-i.; Li, G. *Anal. Chem.* **2017**, *89*, 10776−10782.
(25) Yao, H.-W.; Zhu, X.-Y.; Guo, X.-F.; Wang, H. *Anal. Chem.* **2016**, *88*, 9014−9021.
(26) Lee, M. H.; Jeon, H. M.; Han, J. H.; Park, N.; Kang, C.; Sessler, J. L.; Kim, J. S. *J. Am. Chem. Soc.* **2014**, *136*, 8430−8437.
(27) Chu, H.; Zhao, J.; Mi, Y.; Zhao, Y.; Li, L. *Angew. Chem., Int. Ed.* **2019**, *58*, 14877−14881.
(28) Zhao, J.; Chu, H.; Zhao, Y.; Lu, Y.; Li, L. *J. Am. Chem. Soc.* **2019**, *141*, 7056−7062.
(29) Wang, N.; Yu, X.; Zhang, K.; Mirkin, C. A.; Li, J. *J. Am. Chem. Soc.* **2017**, *139*, 12354−12357.
(30) Chu, H.; Zhao, J.; Mi, Y.; Di, Z.; Li, L. *Nat. Commun.* **2019**, *10*, 2839.
(31) Di, Z.; Liu, B.; Zhao, J.; Gu, Z.; Zhao, Y.; Li, L. *Sci. Adv.* **2020**, *6*, No. eaba9381.
(32) Zhao, J.; Li, Y.; Yu, M.; Gu, Z.; Li, L.; Zhao, Y. *Nano Lett.* **2020**, *20*, 874−880.
(33) Zhao, J.; Gao, J.; Xue, W.; Di, Z.; Xing, H.; Lu, Y.; Li, L. *J. Am. Chem. Soc.* **2018**, *140*, 578−581.
(34) Shao, Y.; Zhao, J.; Yuan, J.; Zhao, Y.; Li, L. *Angew. Chem., Int. Ed.* **2021**, *60*, 8923−8931.
(35) Zhang, X.; Chen, W.; Xie, X.; Li, Y.; Chen, D.; Chao, Z.; Liu, C.; Ma, H.; Liu, Y.; Ju, H. *Angew. Chem., Int. Ed.* **2019**, *58*, 12117−12122.
(36) Song, E.; Cheng, D.; Song, Y.; Jiang, M.; Yu, J.; Wang, Y. *Biosens. Bioelectron.* **2013**, *47*, 445−450.
(37) Wang, Z.; Li, X.; Feng, D.; Li, L.; Shi, W.; Ma, H. *Anal. Chem.* **2014**, *86*, 7719−7725.
(38) Cao, S.; Li, Z.; Zhao, J.; Chen, M.; Ma, N. *ACS Sens.* **2018**, *3*, 1522−1530.
(39) Boonrao, M.; Yodkeeree, S.; Ampasavate, C.; Anuchapreeda, S.; Limtrakul, P. *Arch. Pharmacal Res.* **2010**, *33*, 989−998.
(40) Zhao, W.; Pan, Y.; Wu, J.; Cai, M.; Tian, Y.; Xu, H.; Yu, L.; Wang, H. *Anal. Methods* **2014**, *6*, 7689−7694.
(41) Shi, H.; Sun, Y.; Yan, R.; Liu, S.; Zhu, L.; Liu, S.; Feng, Y.; Wang, P.; He, J.; Zhou, Z.; Ye, D. *Nano Lett.* **2019**, *19*, 937−947.
(42) Chan, Y.-C.; Chen, C.-W.; Chan, M.-H.; Chang, Y.-C.; Chang, W.-M.; Chi, L.-H.; Yu, H.-M.; Lin, Y.-F.; Tsai, D. P.; Liu, R.-S.; Hsiao, M. *Bioelectron* **2016**, *80*, 131−139.
(43) Matsushita, T.; Matsui, Y.; Ikekame, S.; Sakuma, M.; Shirasaki, N. *Environ. Sci. Technol.* **2017**, *51*, 4541−4548.
(44) Lei, Z.; Zhang, H.; Wang, Y.; Meng, X.; Wang, Z. *Anal. Chem.* **2017**, *89*, 6749−6757.
(45) Cho, H.-J.; Lee, S.; Park, S.-J.; Lee, Y.-D.; Jeong, K.; Park, J. H.; Lee, Y.-S.; Kim, B.; Jeong, H.-S.; Kim, S. *Colloids Surf., B* **2019**, *179*, 9−16.
(46) Jezierska, A.; Motyl, T. *Med. Sci. Monit.* **2009**, *15*, RA32−RA40.
(47) Miampamba, M.; Liu, J.; Harootunian, A.; Gale, A. J.; Baird, S.; Chen, S. L.; Nguyen, Q. T.; Tsien, R. Y.; González, J. E. *Theranostics* **2017**, *7*, 3369−3386.

https://doi.org/10.1021/acs.analchem.1c00469
Anal. Chem. 2021, 93, 7258−7265